

## Fullerene-structured nanowires of silicon

Bjorn Marsen and Klaus Sattler

*Department of Physics and Astronomy, University of Hawaii, 2505 Correa Road, Honolulu, Hawaii 96822*

(Received 21 May 1999)

Silicon vapor from a magnetron sputter source was deposited onto highly oriented pyrolytic graphite, resulting in the formation of nanoscale wires. The structures were analyzed by scanning tunneling microscopy. The wires are from 3 to 7 nm in diameter and at least 100 nm long. They tend to be assembled parallel in bundles. In order to understand the observed quasi-one-dimensional structures, diamondlike and fullerenelike wire models are constructed. Molecular-orbit calculations yield binding energies and band gaps of such structures, and lead us to propose a fullerene-type  $\text{Si}_{24}$ -based atomic configuration for nanowires of silicon. [S0163-1829(99)02740-X]

### INTRODUCTION

Semiconductor whiskers, such as Si,<sup>1,2</sup> Ge,<sup>3,4</sup> GaP,<sup>5</sup> GaAs,<sup>1,6,7</sup> and InAs,<sup>8</sup> have been widely studied over the past 25 years because of their unique growth behavior and crystal structures. The studies became possible after Wagner and Ellis<sup>2</sup> had proposed the vapor-liquid-solid model for Si whisker growth using Au as a growth catalyst.

More recently, semiconductor wires thinner than 100 nm have attracted much attention because of their fascinating quantum properties. It has been suggested that they may be used for developing one-dimensional (1D) quantum wire high-speed field effect transistors and light-emitting devices with extremely low power consumption. Sakaki<sup>9</sup> calculated, that for 1D GaAs channels the electron mobility exceeds  $10^6 \text{ cm}^2/\text{V}$  at low temperature, which is more than one order of magnitude larger than the calculated electron mobility of a two-dimensional electron gas.<sup>10</sup> The effect of quantum confinement in quantum wires (QWR's) has been evidenced in the luminescence,<sup>11-13</sup> two-photon optical absorption,<sup>14</sup> inelastic light scattering,<sup>15</sup> and various other studies. It is obvious that impurity scattering and boundary effects become increasingly important when the width of the QWR's is reduced. Also the atomic structure of the QWR's is fundamentally important for their overall properties. In many studies the atomic structure of QWR's has been assumed to be the same as in the crystalline bulk.

Quantum wires of silicon have attracted much attention just recently. In addition to theoretical studies of electronic and optical properties,<sup>16</sup> a number of experimental studies has been reported: transmission electron microscopy,<sup>17</sup> electron transport,<sup>18</sup> photoluminescence,<sup>19,20</sup> infrared-induced emission,<sup>21</sup> and Raman spectroscopy.<sup>19,22</sup> However, the atomic structure of the wires in these studies was not known, and was assumed to be either amorphous or to have the diamond structure of the bulk. This may be justified when the wires are formed by methods like lithography and orientation-dependent etching.<sup>23</sup> However, it may not apply to self-forming quantum wires which were grown freely by vapor condensation. On the nanometer size scale, (meta)stable structures may form, which differ significantly from the crystalline bulk.

Crystalline silicon does not have any tendency to grow in

one dimension, as there is no preferential direction associated with the diamond-type lattice. The formation of  $sp^3$  bonds in silicon leads to fourfold coordination with four equivalent directions for growth. This is in contrast to carbon, which can also occur in  $sp^1$  and  $sp^2$  configurations, and therefore has various forms of 1D structures. As small clusters, carbon grows in the form of linear chains or monocyclic rings. It grows in form of nanotubes<sup>24</sup> having a quasi-1D structure. Such quasi-1D structures are of great interest for scientists and engineers due to their exceptional quantum properties not found in the 3D bulk.

Due to the technological importance, efforts have been made to produce nanometer-scale silicon wires in a controlled manner, using common semiconductor processing steps.<sup>25-28</sup> Quite surprisingly, columns with small diameters have been found after electrochemical treatment of Si wafers with hydrofluoric acid (porous Si).<sup>29,30</sup> There has been much discussion about whether quantum confinement in these wires explains the visible photoluminescence of porous silicon.

Individual nanowires of silicon have been produced by a number of methods,<sup>23,26,27,31-42</sup> for example by natural masking,<sup>32</sup> lithography,<sup>23,38</sup> wet-chemical etching,<sup>34,27</sup> and vapor-liquid-solid growth.<sup>35</sup> These methods use growth techniques which lead to natural surface passivation of the wires, usually by oxidation. Silicon is very easily oxidized, because the diamond-type crystal structure leads to a high density of dangling bonds at the surface. In most studies of silicon nanoparticles and nanowires the dangling surface states were passivated. This leads to nanostructures with a crystalline silicon core surrounded by an amorphous silicon oxide layer. With decreasing size, the surface layer becomes increasingly important for the particle's properties. Consequently it becomes increasingly difficult to interpret the outcome of experiments, as both the particle core and the surface layer (or only one of the two) may be responsible for the observed effects. Therefore, in order to study silicon nanostructures in their pristine form, one needs to make sure that clean conditions are applied during their growth. This is achieved by growth of the structures in ultrahigh vacuum.

We report the formation of silicon nanowires grown from the atomic vapor in UHV. The atomic silicon vapor is deposited onto the (1000) basal plane of single-crystal graphite.

The structures are analyzed by scanning tunneling microscopy. We address the question why quasi-1D structures grow for silicon by suggesting several wire structures. These are investigated by self-consistent-field molecular-orbit calculations (PM3) to find the most stable one.

### EXPERIMENT

Highly oriented pyrolytic graphite (HOPG) was used as substrate because it is chemically inert, with perfect crystal structure being atomically flat over micrometer dimensions. The substrate was prepared by cleavage of HOPG in UHV prior to the deposition. Silicon was then deposited by magnetron sputtering at room temperature. The base pressure of the vacuum chamber was  $10^{-9}$  torr. For the deposition an argon pressure of 8 mtorr was established. The sputtering process took place at a voltage of 600 V, the discharge current was 200 mA. For 120 s, the HOPG sample was exposed to the sputter source. Without breaking the vacuum, the sample was transferred to the scanning tunneling microscope, which is operated at  $2 \times 10^{-10}$  torr.

The interaction of the silicon vapor with the substrate is found to be very small. The graphite substrate does not have dangling surface states and is chemically inert for many adlayer materials. For example, electron-energy-loss spectroscopy studies have shown that K and Cs adsorbates are not influenced by the graphite substrate.<sup>43,44</sup> This is explained by graphite being a semimetal with a nearly zero density of states at the Fermi level. The adlayers are only kept on the surface by weak dipole forces. Transition metals tend to couple stronger to the graphite surface. For adsorbed platinum particles we have observed periodic charge-density modulations close to the adsorption sites.<sup>45</sup> Such modulations are interference patterns for electron waves which are scattered at the altered potential in the substrate surface at an adsorption site. For Pt deposition the thickness of the film deposited on graphite was comparable to the thickness measured with a quartz-crystal monitor. This shows that the sticking coefficient for Pt on HOPG is nearly 1. For silicon adsorption on HOPG, however, the sticking coefficient is very small, which is seen from a markable difference in the film thicknesses of HOPG and the quartz-crystal monitor. Also, for silicon we did not observe superstructures on the support surrounding the adlayers, which additionally indicates that there is very little interaction with the substrate. This weak interaction also leads to the fact that silicon does not wet the HOPG surface. If we deposit very small amounts of silicon we obtain small clusters and particles which are very compact, with spherical shapes, which shows that the substrate is not having any major effect on the particle structure. Initially, the vapor is hot and the adsorbed atoms can freely diffuse along the surface. Subsequently, they can form clusters and larger nanostructures by quasifree nucleation and growth. In the far submonolayer range the growth leads to the formation of small clusters, nanoparticles, and other compact and ordered nanostructures. When growth conditions like exposure time, vapor deposition rate, or substrate temperature are varied, this may sensitively affect the type of structure which forms. The conditions given above turned out to be suitable for the formation of silicon nanowires.

When hot vapor is rapidly quenched on an inert substrate,

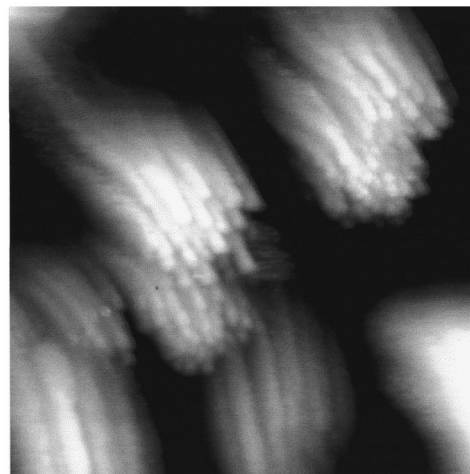


FIG. 1. Several bundles of silicon nanowires (STM image, scan size  $114 \times 114 \text{ nm}^2$ ). Each bundle consists of 20–30 nanowires.

generally amorphous structures tend to form. However, on the nanometer-size scale, such structures may well be ordered. If the ordered areas are very small and if different structural isomers are present on the same sample, this cannot be seen in (x-ray or electron) diffraction experiments. These techniques probe large areas of a sample, and yield an average over individual nanostructures. The result is a superposition of various structures and the adlayer may appear to be amorphous even though it is not. For a nanoscopic characterization the study of individual clusters and nanostructures is required.

We may ask if the observed structures could be due to SiC or C, rather than to pure silicon. In fact, carbon vapor has been found to form nanotubes after being deposited on HOPG.<sup>24</sup> Also, carbon nanotubes tend to form bundles in vapor-phase condensation.<sup>46</sup> Highly oriented pyrolytic graphite is an inert substrate for most materials. On this substrate we have studied clusters of metals,<sup>47–49</sup> carbon,<sup>50</sup> and silicon.<sup>51</sup> It is generally assumed that no chemical bonds are formed between cluster and HOPG support and that the adlayers are coupled to the substrate by physisorption only. This is supported by our observations of extremely small sticking coefficients. By comparison of the deposited amount with the rate at a quartz-crystal monitor we find that only a small fraction ( $10^{-2} - 10^{-3}$ ) of the silicon vapor remains at the HOPG substrate. If chemical bonds were formed between Si atoms and HOPG, a high sticking coefficient would be expected. Therefore, we conclude that the formation of SiC structures does not occur. It also would require the graphite substrate to completely dissolve in the adsorption area with strong distortions of the surrounding graphite lattice. However, in atomic resolution images we find that the graphite lattice is undistorted around silicon adlayer structures. Therefore we conclude that the linear structures which we observe are due to pure silicon.

### RESULTS AND DISCUSSION

A STM image ( $114 \times 114 \text{ nm}^2$ ) of silicon nanowires is displayed in Fig. 1. The picture shows several bundles with 20–30 wires per bundle. The nanowires are more than 100 nm long, with diameters from 3 to 7 nm. The width of the

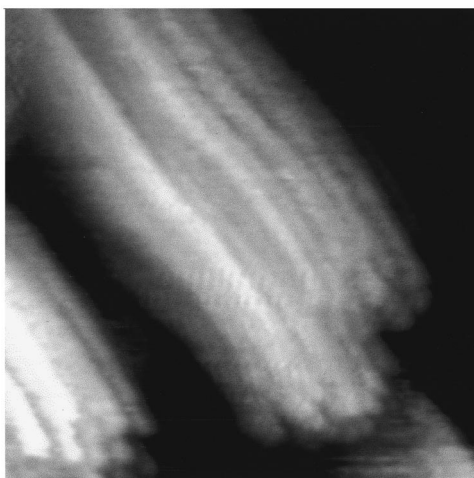


FIG. 2. Si nanowires in a bundle showing a slight curvature (STM image, scan size  $77 \times 77 \text{ nm}^2$ ). The wires are more than 100 nm long.

wires is very uniform in each bundle. A section ( $77 \times 77 \text{ nm}^2$ ) of the image is shown in Fig. 2. The nanowires are tightly packed in the bundle. While the wires are linearly aligned with most bundles they occasionally are slightly bent. This is seen for the bundle in Fig. 2. Another area on the sample is displayed in Fig. 3 ( $67 \times 67 \text{ nm}^2$ ), where three bundles can be seen. The image shows that the wires have about the same diameter within each bundle. The average wire diameters are 3, 4, and 7 nm in the bundles assigned with *a*, *b*, and *c*, respectively. Figure 4 shows cross-sectional plots for the three bundles. The cylindrical shapes of the wires cannot directly be seen, as the STM does not image the undercut part of a cylindrical object. However, the profile shows the rounded top portion of the wires. The cross section of bundle *a* is not round and its surface is quite flat. Other bundles rather show rounded surface profiles [Figs. 4(b) and 4(c)], which indicates cylindrical shapes of the bundles. The diameter of the wires can be determined from the apparent width taken from the STM images or from the nearest-neighbor distance in the bundles. The apparent width of a wire depends on the curvature of the STM tip and also

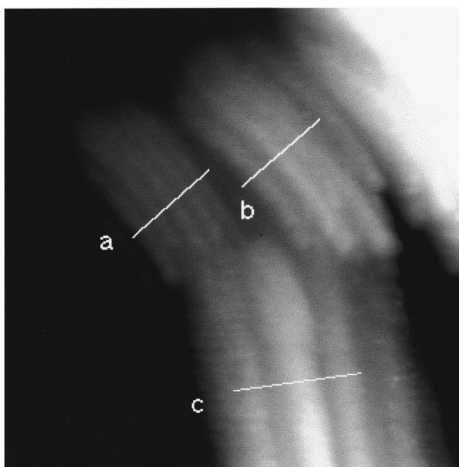


FIG. 3. Three bundles of silicon nanowires with different diameters (STM image, scan size  $67 \times 67 \text{ nm}^2$ ).

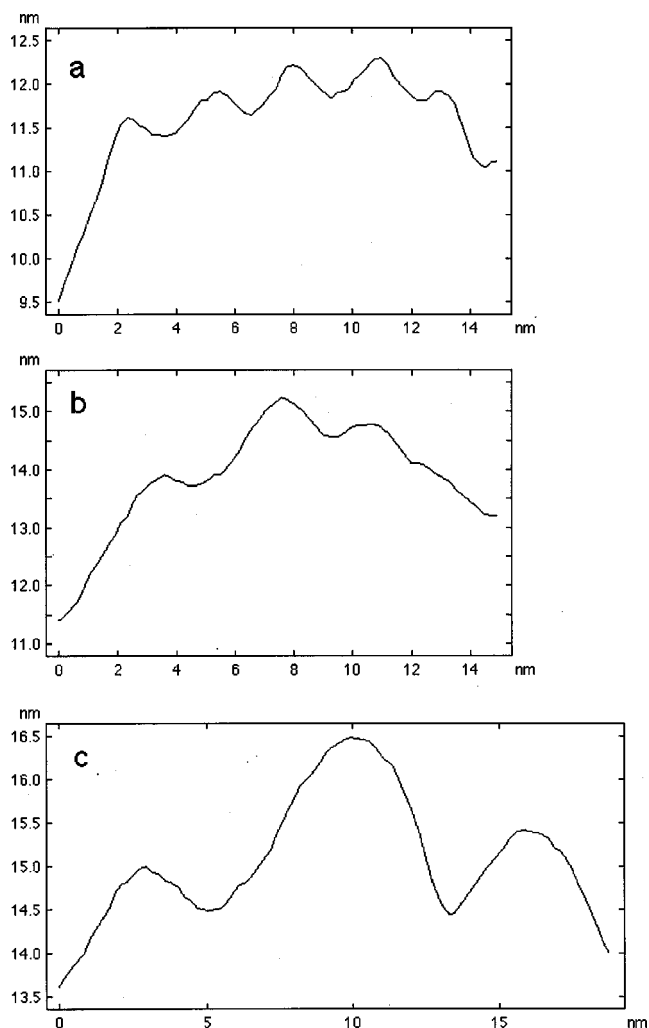


FIG. 4. Profiles of the three bundles of Fig. 3. From the wire separations the diameters are estimated to be (a) 3 nm, (b) 4 nm, and (c) 7 nm.

on the area of the wire which is exposed and not hidden by its neighbors in the bundle. The repeat distance of the wires in a bundle, however, is independent of the form of the tip, and its measurement usually gives much better values for wire diameters.

We have observed nanowires on several samples which were prepared in similar ways. Most of the wires were aligned parallel in bundles. We explain this with the tendency of the wires to saturate their dangling surface states by forming bonds between wires in a bundle. The coupling between the wires in a bundle must be very effective because the  $sp^3$ -type hybrids of silicon form very strong bonds once they overlap. Only occasionally we found individual wires located on the bare graphite surface and not being assembled in bundles.

It is evident that one has to look for an alternative to the 3D diamond structure to understand why silicon vapor may grow in the form of wires. We start from the requirement of a distinct wire axis, and keep bond angles close to the bulk ones. Also we apply the topological restrictions that only five- and six-membered rings may occur. Other-membered rings yield highly strained networks inconsistent with suitable bond angles for silicon. Also, we did not consider gra-

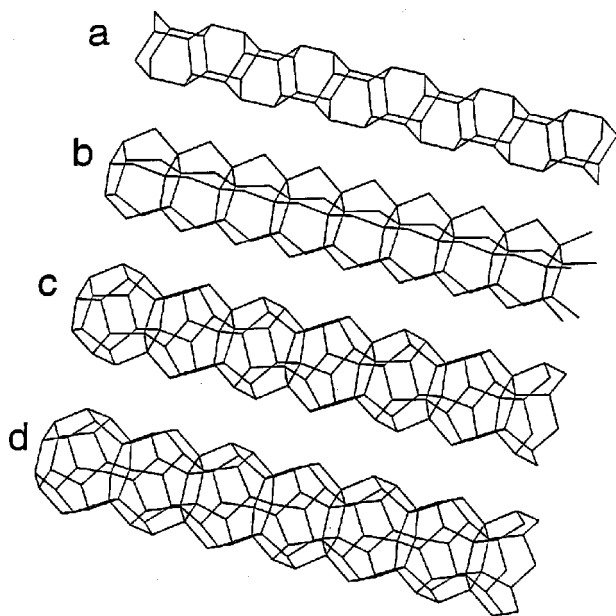


FIG. 5. Four models of possible nanowire core structures. (a)  $\text{Si}_{12}$  cage polymer. (b)  $\text{Si}_{15}$  cage polymer. (c)  $\text{Si}_{20}$  cage polymer. (d)  $\text{Si}_{24}$  cage polymer.

phitic nanotube structures. Graphene atomic layers are  $sp^2$ -type networks and are unlikely to form for silicon. Taking into account the above considerations, we construct several linear polyhedral networks: (a)  $\text{Si}_{12}$ -cage polymer structure (12 atoms per unit cell), (b)  $\text{Si}_{15}$ -cage polymer structure (ten atoms per unit cell), (c)  $\text{Si}_{20}$ -cage polymer structure (based on the  $I_h$  dodecahedron, 30 atoms per unit cell), and (d)  $\text{Si}_{24}$ -cage polymer structure (based on the  $D_{6d}$  icosahedron, 36 atoms per unit cell).

The suggested structures are shown in Fig. 5. All models have in common a stacking of Si cages, in the center of which lies the wire axis. While these lattices deviate significantly from the diamond-structured bulk, tetrahedral configuration of the Si atoms is maintained. Some of the properties of the wires are summarized in Table I.

In structure *a* ( $C_{3v}$  symmetry), the axis of the wire passes through the centers of buckled  $\text{Si}_6$  rings. Two adjacent rings are connected by three bonds and form a  $\text{Si}_{12}$  cage. This cage represents the unit cell, which is repeated every 6.31 Å. The surface of the wire consists of buckled hexagons.

Structure *b* ( $C_{5v}$  symmetry) consists of planar pentagons, joined through five outward oriented interstitial atoms. Two pentagons together with the interstitial atoms form a cage. The unit cell of this structure contains ten atoms, and the repeat distance is 3.84 Å. The surface of the wire consists of buckled hexagons.

TABLE I. Properties of the investigated wire structures.

Model	Symmetry	Atoms per unit cell	$N_{DB}^a$	$E_B$ (eV) <sup>b</sup>
a	$C_{3v}$	12	1	3.23
b	$C_{5v}$	10	3/2	3.28
c	$C_{5v}$	30	2/3	3.63
d	$C_{6v}$	36	2/3	3.87

<sup>a</sup>Average number of dangling bonds per atom.

<sup>b</sup>Binding energies for a single cage, from PM3 calculation.

Structure *c* ( $C_{5v}$  symmetry) is built from  $\text{Si}_{20}$  cages. These dodecahedra ( $I_h$  symmetry) are the smallest possible fullerene structures, consisting of 12 pentagons. In the wire structure, two adjacent cages share one pentagon. The 30 atoms of  $1\frac{1}{2}$  such cages build the unit cell, which is repeated every 9.89 Å. Pentagons make up the surface net of this wire.

Structure *d* ( $C_{6v}$  symmetry) is similar to structure *c*, except that  $\text{Si}_{24}$  cages ( $D_{6d}$  symmetry) are used as building blocks. These units contain 12 pentagons and two hexagons. The hexagons are shared by two adjacent cages and are concentric to the wire axis. The unit cell consists of 36 atoms, and the lattice parameter is 10.03 Å. The surface of the wire consists of pentagons.

The  $\text{Si}_{20}$  and  $\text{Si}_{24}$  cages correspond to the smallest fullerenes.  $\text{Si}_{20}$  is a 12-hedron consisting entirely of pentagons. It has six equivalent fivefold symmetry axes. The fullerene 13-hedron ( $\text{Si}_{22}$ ) does not exist. The fullerene 14-hedron ( $\text{Si}_{24}$ ) has twofold linear ( $30^\circ$  twisted) coordination. In the case of carbon, these small fullerenes are not found in experiments. In fact, Kroto argued that the smaller the number of isolated pentagons, the more stable the fullerene.<sup>52</sup> A fullerene consisting entirely of fused pentagons is therefore the least stable in the case of carbon. This ‘‘isolated pentagon rule’’ (IPR) may be applied to carbon but not to silicon. Conversely, the smallest fullerenes are the most stable ones in the case of silicon. If there are fused pentagons, the atoms sharing two or three pentagons have bond angles of  $108^\circ$  which is very close to the ideal  $sp^3$  angle ( $109.5^\circ$ ). While carbon is flexible with the type of hybridization ( $sp^3$ ,  $sp^2$ , and  $sp^1$ ), silicon is restricted to  $sp^3$ . Therefore, a fused pentagon rule seems to be valid for silicon. This rule would state for a fullerene silicon network, that the larger the number of fused pentagons, the more stable the structure is. Therefore, in the silicon-based fullerene family, the  $\text{Si}_{20}$  cluster should have the largest binding energy.

One condition for growth of a cage-based wire seems to be that the cage has one symmetry axis which is different from the others. This is given for structures *b* and *d*, but not for *a* and *c*. With structures *a* and *c*, the cages consist of either only hexagons or only pentagons, respectively. Starting from these cages, further growth may proceed in all directions, leading to 3D structures. This is different for structures *b* and *d*. Structure *b*, for example, has pentagons at opposite sides, and otherwise hexagons, and therefore the cage of structure *b* has one direction specified along which further growth may continue preferentially. A second cage can be attached along this direction so that again the pentagon is positioned along the axis. Further cages can form in the same way, building up the wire. The cage of structure *d* has also one direction specified. The  $\text{Si}_{24}$  cage has two hexagons on opposite sides, and otherwise only pentagons. The atomic net is anisotropic with one direction specified along which further growth can proceed preferentially. For both wires, *b* and *d*, the quasi-1D growth would continue straight rather than zigzag. We conclude that structures *b* and *d* are possible candidates for silicon nanowires.

In order to find the most stable of the proposed structures we calculated their binding energies and highest occupied–lowest unoccupied molecular-orbital (HOMO–LUMO) gaps. We employ the PM3 self-consistent-field molecular-orbital

TABLE II. Comparison of calculated binding energies per atom for  $\text{Si}_3$ – $\text{Si}_7$ . All binding energies are in eV.

$N$	PM3 (present results)	<i>Ab initio</i> (Ref. 54)	TB-MD (Ref. 55)
3	2.50	2.54	2.63
4	2.99	3.17	3.08
5	3.24	3.30	3.43
6	3.58	3.60	3.74
7	3.74	3.80	3.85

theory derived by Stewart.<sup>53</sup> PM3 is a well-established iterative quantum-mechanical technique giving excellent results for organic molecules. In order to use this theory for nanowires of silicon, we first tested the method's ability to reveal reasonable results for clusters. We calculated binding energies for small Si clusters ( $\text{Si}_3$  to  $\text{Si}_7$ ) and obtained excellent agreement with both *ab initio*<sup>54</sup> and tight-binding molecular-dynamics<sup>55</sup> calculations. The data are given in Table II. The results demonstrate that PM3 is capable to yield good results for small structures of silicon.

We first calculated the binding energies per atom for the individual cages of the wire structures *a*–*d* (Table I). The values lie between 3.23 and 3.87 eV. Then we added more cages forming the wires. In Fig. 6, the binding energies are plotted for wires of various lengths. We find that the atoms in longer wires are bound more strongly. The binding energies saturate at relatively small cluster sizes, for example at about  $n=30$  (3.6 eV) for structure *a*. Clearly, the diamond-type wires (*a* and *b*) have binding energies which are much smaller than the fullerene-type wires (*c* and *d*).

For small length, structure *d* has the highest binding energy. The  $\text{Si}_{24}$  fullerene cage is thermodynamically favorable over the other structures, and also has a symmetry axis specified for preferential addition of further cages. Therefore, the  $\text{Si}_{24}$ -based wire may have the best chance to form.

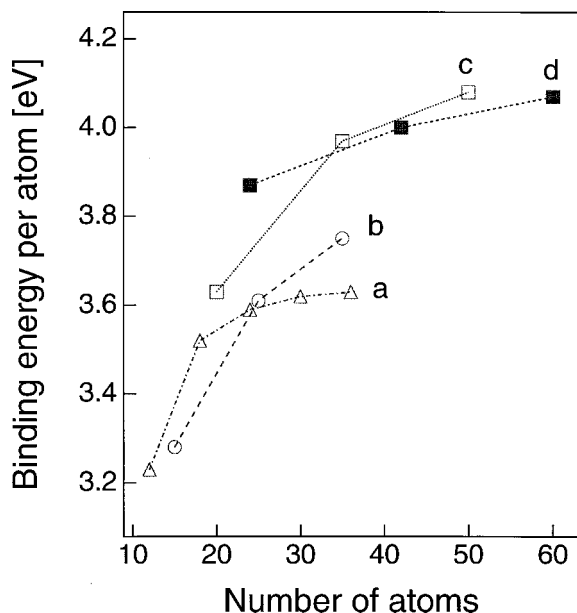


FIG. 6. Binding energies obtained from PM3 calculations as a function of size for the suggested models. The points are connected to guide the eye.

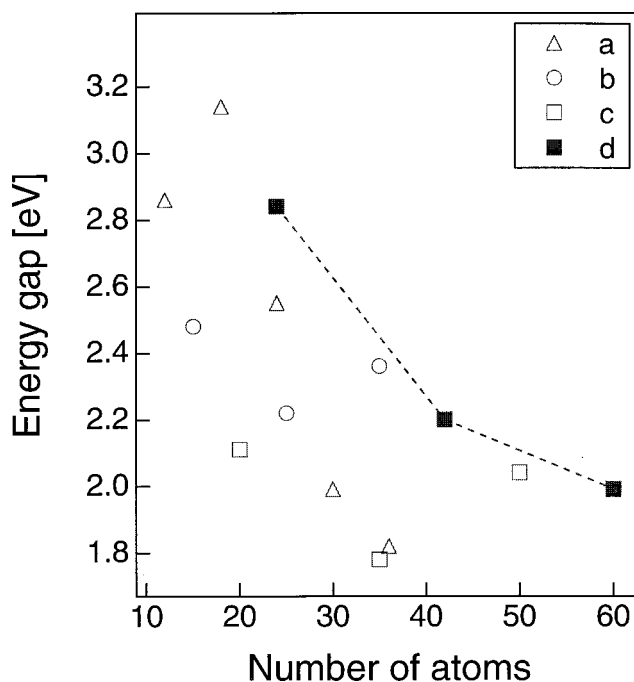


FIG. 7. PM3-calculated energy gaps as a function of size for the suggested models. For a given size, the energy gap of structure (*d*) is highest.

The width of the HOMO-LUMO gap can be another indicator for the stability of a nanostructure. Our calculations show energy gaps between 1.8 and 3.2 eV, for the wires of Fig. 5, when containing up to 60 atoms. The wires are between  $\sim 4$  (structure *a*) and  $10 \text{ \AA}$  (structure *d*) thick. The gap becomes rapidly smaller with increasing length of the wire (Fig. 7). For a given size, the energy gap of structure *d* is largest.

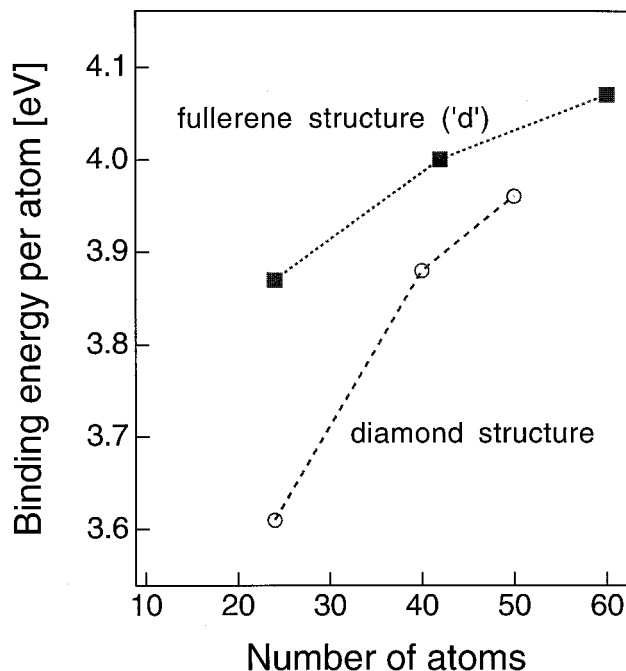


FIG. 8. Comparison of the PM3 binding energies for model (*d*) and for similarly sized diamond structure bulk fragments. For a given size the fullerene structure is energetically favorable.

We conclude that among the four considered configurations, structure *d* has the highest binding energy per atom and the largest energy gap. If energetics is responsible for the wire formation in its early stage, then structure *d* should grow preferentially. Once the  $\text{Si}_{24}$ -based polymer has formed, the wire may continue to add layer by layer, further increasing its diameter.

A crucial question remains, whether structure *d* is favorable over the diamond structure of the bulk. To study this question, we constructed 3D silicon clusters with a diamond structure and calculated their binding energies. We find that at this small size, the binding energies of  $\text{Si}_{24}$ -based wires are higher than those of equally sized diamond-structure bulk fragments (Fig. 8).

Only a few studies have explored the possibility of fullerene structures for silicon clusters.<sup>56–58</sup> Dodecahedral  $\text{Si}_{20}$  clusters were predicted to be stable, using a model potential for  $sp^3$ -hybridized atoms.<sup>56</sup> It has been argued that these clusters may not be found isolated in experiments because the dangling bonds (on the cages' outer surfaces) would make them "unextractable"<sup>57</sup> from other silicon material. Fullerenic  $\text{Si}_{20}$  units were recently synthesized as bulk bcc solids, with additional Si atoms at half the interstitial sites (three sites per  $\text{Si}_{20}$ ), leading to a silicon lattice with  $(\text{Si}_3\text{Si}_{20})_2$ , which is equal to  $\text{Si}_{46}$  units.<sup>58</sup> Such hollow silicon materials may have various interesting properties. In fact, superconductivity was found recently in the  $\text{Na}_2\text{Ba}_6\text{Si}_{46}$  phase.<sup>58</sup>

The cage structure has not been considered for small silicon clusters until recently. In early theoretical studies it was assumed that there are two basic structures for small silicon particles: a compact close-packed structure for very small clusters and a diamond-type structure for large particles. An important issue in calculations of silicon clusters was to determine the critical size at which the cluster structure changes from compact (with high coordination) to the more open diamond structure with covalent bonds. Phillips<sup>59–61</sup> concluded from analyzing fragmentation and ionization experiments<sup>62,63</sup> that silicon clusters with sizes smaller than 10 have a unique structure with no resemblance to the diamond lattice. For larger clusters, he assumed the structure of covalently bonded fragments of the bulk. These early conclusions were later confirmed by detailed quantum-mechanical calculations which showed indeed that silicon clusters up to  $n=10$  do not look like bulk fragments but rather have a high coordination structure.<sup>54,64–66</sup> The critical size for the transition from high to low coordination was calculated but with very different results, ranging from  $n=50$  (Ref. 67) to  $n=4200$ .<sup>68,69</sup> Along with a transition in structure, a transition in shape has also been predicted. Simulations using a classical interatomic force field indicate that silicon clusters of size smaller than 25 tend to be prolate, whereas larger clusters tend to be oblate.<sup>70,71</sup> This prediction was later confirmed experimentally,<sup>72–74</sup> showing a transition at sizes between 24 and 27; clusters with less than 24 atoms were found to be prolate, whereas clusters larger than 27 atoms were found to be oblate. The transition was further investigated by optimizing surface reconstruction in larger clusters.<sup>75</sup>  $\text{Si}_{24}$  did not appear to be exceptional in earlier studies, in mass spectra, fragmentation pattern, etc. For the growth of nanowires, however, it seems to play an excep-

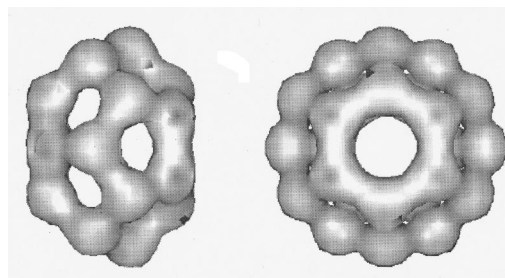


FIG. 9. Charge density isosurface of the fullerenic  $\text{Si}_{24}$ .

tional role. We consider it as the nucleation seed which has the growth axis built in.

In theoretical studies of silicon quantum wires the diamond structure has been assumed for very thin wires with cross sections of  $3 \times 3$ ,  $4 \times 4$ , and  $5 \times 5$  atoms, and diameters between 0.77 and 1.53 nm.<sup>76</sup> This, however, may not have been appropriate. For such small diameters, the diamond lattice does not appear to be the lowest-energy structure. Also, the assumption of the bulk crystal structure does not take into account the question of linear growth. A small Si crystallite with diamond structure is isotropic, and there is no reason why it should continue to grow just in one direction. Instead, a  $\text{Si}_{24}$ -based wire has an anisotropy built into its  $\text{Si}_{24}$  nucleation seed.

In Fig. 9 the charge-density distribution of  $\text{Si}_{24}$  is shown, as obtained from the PM3 analysis. The left side of the figure gives a side view with the pentagonal-type surface. The axis for wire growth goes through the two hexagons on the opposite sides of the cluster. The hexagons are rotated by  $30^\circ$  relative to each other. On the right side of the figure, the cluster is viewed from the wire axis. It can be seen that the charge-density distribution is more uniform within the hexagonal rings compared to that in the pentagonal rings. This indicates that the probability for further growth is different along the wire axis compared to the pentagonal surface. As the diameters of the observed nanowires are larger than the diameter of  $\text{Si}_{24}$ , we may consider two processes with different growth speeds: (i) growth along the wire axis, and (ii) surface layer growth. For the structure to form of a wire the growth has to proceed faster along the axis than on the surface. At this stage, our analysis is still open to question why growth would proceed faster at hexagonal compared to pentagonal rings.

The two hexagons in the otherwise pentagonal network are at opposite sides of the  $\text{Si}_{24}$  cluster, which makes the cluster's surface anisotropic for the addition of further atoms. Of all possible fullerene-type cages, the 24-atom cage is the only one which has this property. The fullerene-structure family starts with a cage of 20 atoms. The 20-atom cage (the pentagonal dodecahedron) is isotropic, in having a surface net entirely made of pentagons. With 22 atoms one cannot construct a closed 5/6 network; therefore, a  $\text{Si}_{22}$  cluster does not exist in form of a fullerene-type cage. Cages with more than 24 atoms can be constructed by addition of two atoms each, leading to the cluster series  $\text{Si}_{26}, \text{Si}_{28}, \text{Si}_{30}$ , etc. Each of these cages consists of 12 pentagons (which follows Euler's description of closed 5/6 networks) and increasing numbers of hexagons with increasing size, with  $\text{Si}_{26}, \text{Si}_{28}, \text{Si}_{30}$ , etc.

having three, four, five, etc. hexagons, respectively. These clusters are not candidates for nucleation seeds of nanowires as they have no growth axis built in. The  $\text{Si}_{24}$  cluster is the only one with this property and therefore appears to be the seed for the core of a silicon nanowire.

We note that there is an intriguing similarity in the STM images of silicon nanowires and carbon nanotubes. In earlier studies we have produced carbon nanotubes by vapor phase growth,<sup>24</sup> with a method being very similar to the one used for silicon. The tubes were grown on the HOPG surface in UHV by quenching the vapor. The only difference was that the carbon vapor was produced by a hot carbon foil at  $\sim 3400^\circ\text{C}$  and not by magnetron sputtering as for silicon. Otherwise the procedures were the same for both materials. We conclude that both silicon and carbon can form linear nanowires by growth from the vapor. In the case of carbon we could determine the graphitic structure of the tubes directly by atomic-resolution scanning tunneling microscopy.<sup>24</sup> For silicon nanowires, however, we did not obtain atomic resolution. The surface of the wires appeared rather smooth on the atomic scale. It may be that the overlap of dangling surface states leads to the formation of an energy band at the surface of the wire, making the surface metallic with electron states smeared out in space.

We have shown in this paper that the silicon wires tend to form bundles. In the case of carbon, the tubes also tend to be assembled in bundles.<sup>46</sup> For both materials, the wires have the same diameter in a particular bundle. In another bundle the diameter of the wires may be different, but again uniform within that bundle. It is intriguing that the same behavior occurs both for silicon and carbon. This may be due to the similar dynamics during growth or to favorable energetics for bundles with equally sized nanowires or nanotubes. For both silicon and carbon we observe that the wires are close packed in the bundles. In general, close-packed structures can only form with units which have the same size. Therefore, it appears that during growth of the individual wires, bundles are formed and the energy is simultaneously mini-

mized by the formation and close packing of equally sized wires.

As discussed above, we consider the HOPG substrate to be mostly inert for silicon adlayers. We have found the same for carbon. When carbon vapor is deposited on HOPG, the sticking coefficient is very small, and carbon does not wet the surface. For both materials, the substrate merely acts as a heat sink when the hot vapor is quenched. Due to the layered structure of graphite and its low density of states at the Fermi level the heat conduction is low, which leads to a slow cooling rate for the deposited vapor. Such slow quasifree growth conditions obviously can lead to linear growth both for silicon and carbon. The cooling rate is probably between the two extremes, a slow one and a fast one for the growth of crystalline and amorphous silicon, respectively. Both, silicon nanowires and carbon nanotubes are metastable structures and represent local minima in the potential-energy surface. While both materials can form linear nanowires of similar diameter and are tightly packed in bundles, their atomic structures are very likely not the same. While a carbon nanotube consists of cylindrical layers of graphite, a silicon nanowire likely consists of a fullerene-polymer type core with close-to-cylindrical layers of silicon.

The possibility to grow silicon wires from the vapor in UHV is of fundamental and technological interest. We studied pristine silicon nanowires, and found that the most probable core structure is the one which is based on  $\text{Si}_{24}$  units. After the first unit has nucleated, the growth may proceed preferentially in one direction by forming further  $\text{Si}_{24}$  cages. This growth does not occur in all directions because the  $\text{Si}_{24}$  cage is anisotropic at its surface. The  $\text{Si}_{24}$  fullerene cage is exceptional among fullerene-type structures. It is the only one which consists of just two equal network units. In  $\text{Si}_{24}$ , there are two hexagons in an otherwise pentagonal network. The hexagons are on opposite sides of the cluster, and therefore define a direction which can lead to the addition of further atoms in a nonisotropic way. With a fullerene-type  $\text{Si}_{24}$ -based core, the wires could have exceptional band structure and transport properties.

- 
- <sup>1</sup>E. I. Givargizov, *J. Cryst. Growth* **31**, 20 (1975).  
<sup>2</sup>R. S. Wagner and W. C. Ellis, *Appl. Phys. Lett.* **4**, 89 (1964).  
<sup>3</sup>E. I. Givargizov, *J. Cryst. Growth* **20**, 217 (1973).  
<sup>4</sup>G. A. Boostma and H. J. Gassen, *J. Cryst. Growth* **10**, 223 (1971).  
<sup>5</sup>E. Schoenherr, *J. Cryst. Growth* **9**, 346 (1971).  
<sup>6</sup>K. Himura, T. Katsuiama, K. Ogawa, G. P. Morgan, M. Koguchi, and H. Kakibayashi, *Appl. Phys. Lett.* **59**, 431 (1991).  
<sup>7</sup>M. Fujii, H. Iwanaga, and N. Shibata, *J. Cryst. Growth* **99**, 179 (1990).  
<sup>8</sup>M. Koguchi, H. Kakibayashi, M. Yazawa, K. Hiruma, and T. Katsuyama, *J. Appl. Phys.* **31**, 2061 (1992).  
<sup>9</sup>H. Sakaki, *Jpn. J. Appl. Phys.* **19**, L735 (1980).  
<sup>10</sup>S. Mori and T. Ando, *J. Phys. Soc. Jpn.* **48**, 865 (1980).  
<sup>11</sup>J. Bloch, U. Bockelmann, and F. Laruelle, *Europhys. Lett.* **28**, 501 (1994).  
<sup>12</sup>H. Akiyama, T. Someya, and H. Sakaki, *Phys. Rev. B* **53**, R4229 (1996).  
<sup>13</sup>F. Vouilloz, D. Y. Oberli, M.-A. Dupertuis, A. Gustafsson, F. Reinhardt, and E. Kapon, *Phys. Rev. Lett.* **78**, 1580 (1997).  
<sup>14</sup>R. Cingolani, M. Lepore, R. Tommasi, I. M. Catalano, H. Lage, D. Heitmann, K. Ploog, A. Shimizu, H. Sakaki, and T. Ogawa, *Phys. Rev. Lett.* **69**, 1276 (1992).  
<sup>15</sup>A. R. Goni, A. Pinczuk, J. S. Weiner, B. S. Dennis, L. N. Pfeiffer, and K. W. West, *Phys. Rev. Lett.* **70**, 1151 (1993).  
<sup>16</sup>A. M. Saitta, F. Buda, and P. V. Giaquinta, *Phys. Rev. B* **53**, 1446 (1996).  
<sup>17</sup>G. W. Zhou, Z. Zhang, and D. P. Yu, *Appl. Phys. Lett.* **73**, 677 (1998).  
<sup>18</sup>V. Ng, H. Ahmed, and T. Shimada, *Appl. Phys. Lett.* **73**, 972 (1998).  
<sup>19</sup>D. Papadimitriou and A. G. Nassiopoulou, *J. Appl. Phys.* **84**, 1059 (1998).  
<sup>20</sup>D. P. Yu, Z. G. Bai, and S. Q. Geng, *Phys. Rev. B* **59**, R2 498 (1999).  
<sup>21</sup>N. T. Bagraev, E. T. Chaikina, and A. M. Malyarenko, *Solid-State Electron* **42**, 1199 (1998).  
<sup>22</sup>B. Li, D. Yu, and S.-L. Zhang, *Phys. Rev. B* **59**, 1645 (1999).  
<sup>23</sup>H. Namatsu, K. Kurihara, and T. Makino, *Appl. Phys. Lett.* **70**, 619 (1997).

- <sup>24</sup>M. Ge and K. Sattler, *Science* **260**, 515 (1993).
- <sup>25</sup>H. I. Liu, D. K. Biegelsen, F. A. Ponce, N. M. Johnson, and R. F. W. Pease, *Appl. Phys. Lett.* **64**, 1383 (1994).
- <sup>26</sup>H. Namatsu, Y. Takahashi, M. Nagase, and K. Murase, *J. Vac. Sci. Technol. B* **13**, 2166 (1995).
- <sup>27</sup>Y. Shi, J. L. Liu, F. Wang, Y. Lu, R. Zhang, S. L. Gu, P. Han, L. Q. Hu, Y. D. Zheng, C. Y. Lin, and D. A. Du, *J. Vac. Sci. Technol. A* **14**, 1194 (1996).
- <sup>28</sup>G. S. Chen, C. B. Boothroyd, and C. J. Humphreys, *Appl. Phys. Lett.* **62**, 1949 (1993).
- <sup>29</sup>L. T. Canham, *Appl. Phys. Lett.* **57**, 1046 (1990).
- <sup>30</sup>V. Lehmann and U. Goesele, *Appl. Phys. Lett.* **58**, 856 (1991).
- <sup>31</sup>J. L. Liu, Y. Shi, and Y. D. Zheng, *Appl. Phys. Lett.* **68**, 352 (1996).
- <sup>32</sup>M. Gotza, B. Saint-Cricq, and P.-H. Jouneau, *Microelectron. Eng.* **27**, 129 (1995).
- <sup>33</sup>G. Hashiguchi and H. Mimura, *Jpn. J. Appl. Phys.* **33**, L1649 (1994).
- <sup>34</sup>J. L. Liu, Y. Shi, and Y. D. Zheng, *J. Vac. Sci. Technol. B* **13**, 2137 (1995).
- <sup>35</sup>A. M. Morales and C. M. Lieber, *Science* **279**, 208 (1998).
- <sup>36</sup>T. Ono, H. Saitoh, and M. Esashi, *Appl. Phys. Lett.* **70**, 1852 (1997).
- <sup>37</sup>G. D. Sanders and Y.-C. Chang, *Appl. Phys. Lett.* **60**, 2525 (1992).
- <sup>38</sup>A. G. Nassiopoulou, S. Grigoropoulos, and D. Papadimitriou, *Thin Solid Films* **297**, 176 (1997).
- <sup>39</sup>J. Westwater, D. P. Gosain, and H. Ruda, *J. Vac. Sci. Technol. B* **15**, 554 (1997).
- <sup>40</sup>J. Westwater, D. P. Gosain, and S. Usui, *Phys. Status Solidi A* **165**, 37 (1998).
- <sup>41</sup>S.-i. Yanagiya, S. Kamimura, and H. Koinuma, *Appl. Phys. Lett.* **71**, 1409 (1997).
- <sup>42</sup>D. P. Yu, Z. G. Bai, Y. Ding, Q. L. Hang, H. Z. Zhang, J. J. Wang, Y. H. Zou, W. Qian, G. C. Xiong, H. T. Zhou, and S. Q. Feng, *Appl. Phys. Lett.* **72**, 3458 (1998).
- <sup>43</sup>M. R. Hunt and R. E. Palmer, *Philos. Trans. R. Soc. London, Ser. A* **356**, 231 (1998).
- <sup>44</sup>Z. Y. Li, K. M. Hock, and R. E. Palmer, *Phys. Rev. Lett.* **67**, 1562 (1991).
- <sup>45</sup>J. Xhie, K. Sattler, U. Mueller, G. Raina, and N. Venkateswaran, *Phys. Rev. B* **43**, 8917 (1991).
- <sup>46</sup>M. Ge and K. Sattler, *Appl. Phys. Lett.* **64**, 710 (1994).
- <sup>47</sup>U. Mueller, K. Sattler, J. Xhie, N. Venkateswaran, and G. Raina, *J. Vac. Sci. Technol. B* **9**, 829 (1991).
- <sup>48</sup>E. Ganz, K. Sattler, and J. Clarke, *Phys. Rev. Lett.* **60**, 1856 (1988).
- <sup>49</sup>E. Ganz, K. Sattler, and J. Clarke, *Surf. Sci.* **219**, 33 (1989).
- <sup>50</sup>M. Lonfat, B. Marsen, and K. Sattler, *Chem. Phys. Lett.* (to be published).
- <sup>51</sup>B. Marsen and K. Sattler (unpublished).
- <sup>52</sup>H. W. Kroto, *Nature (London)* **329**, 529 (1987).
- <sup>53</sup>J. J. P. Stewart, *J. Comput. Chem.* **10**, 221 (1989).
- <sup>54</sup>K. Raghavachari, *J. Chem. Phys.* **84**, 5672 (1986).
- <sup>55</sup>M. Menon and K. R. Subbaswamy, *Phys. Rev. B* **47**, 12 754 (1993).
- <sup>56</sup>S. Saito, S. Ohnishi, and S. Sugano, *Phys. Rev. B* **33**, 7036 (1986).
- <sup>57</sup>S. Saito, in *Cluster Assembled Materials*, edited by K. Sattler (Trans Tech, Zuerich, 1996), Vol. 232, p. 233.
- <sup>58</sup>H. Kawaji, H. Horie, S. Yamanaka, and M. Ishikawa, *Phys. Rev. Lett.* **74**, 1427 (1995).
- <sup>59</sup>J. C. Phillips, *J. Chem. Phys.* **88**, 2090 (1988).
- <sup>60</sup>J. C. Phillips, *J. Chem. Phys.* **85**, 5246 (1986).
- <sup>61</sup>J. C. Phillips, *J. Chem. Phys.* **87**, 1712 (1987).
- <sup>62</sup>L. A. Bloomfield, R. R. Freeman, and W. L. Brown, *Phys. Rev. Lett.* **54**, 2246 (1985).
- <sup>63</sup>Y. Liu, Q.-L. Zhang, F. K. Tittel, R. F. Carl, and R. E. Smalley, *J. Chem. Phys.* **85**, 7434 (1986).
- <sup>64</sup>K. Raghavachari and C. M. Rohlfing, *J. Chem. Phys.* **89**, 2219 (1988).
- <sup>65</sup>P. Ballone, W. Andreoni, R. Car, and M. Parrinello, *Phys. Rev. Lett.* **60**, 271 (1988).
- <sup>66</sup>N. Binggeli, *Phys. Rev. Lett.* **68**, 2956 (1992).
- <sup>67</sup>J. R. Chelikowsky, *Phys. Rev. Lett.* **60**, 2669 (1988).
- <sup>68</sup>D. Tomanek and M. A. Schlüter, *Phys. Rev. Lett.* **56**, 1055 (1986).
- <sup>69</sup>D. Tomanek and M. A. Schlüter, *Phys. Rev. B* **36**, 1208 (1987).
- <sup>70</sup>J. R. Chelikowsky, J. C. Phillips, M. Kamal, and M. Strauss, *Phys. Rev. Lett.* **62**, 292 (1989).
- <sup>71</sup>J. R. Chelikowsky, K. Glassford, and J. C. Phillips, *Phys. Rev. B* **44**, 1538 (1991).
- <sup>72</sup>M. F. Jarrold and V. A. Constant, *Phys. Rev. Lett.* **67**, 2994 (1991).
- <sup>73</sup>M. F. Jarrold, *Science* **252**, 1085 (1991).
- <sup>74</sup>M. F. Jarrold and J. E. Bower, *J. Chem. Phys.* **96**, 9180 (1992).
- <sup>75</sup>E. Kaxiras and K. Jackson, *Phys. Rev. Lett.* **71**, 727 (1988).
- <sup>76</sup>T. Ohno, K. Shiraishi, and T. Ogawa, *Phys. Rev. Lett.* **1992**, 2400 (1992).